

E1-2011-52

A STUDY OF RATES OF  $(n, f)$ ,  $(n, \gamma)$ , AND  $(n, 2n)$   
REACTIONS IN  $^{nat}\text{U}$  AND  $^{232}\text{Th}$  PRODUCED  
BY THE NEUTRON FLUENCE IN THE GRAPHITE SETUP  
(GAMMA-3) IRRADIATED BY 2.33 GeV  
DEUTERON BEAM

Submitted to «European Physical Journal A»

J. Adam<sup>1,2\*</sup>, Chitra Bhatia<sup>3</sup>, K. Katovsky<sup>1</sup>, V. Kumar<sup>3,7</sup>, M. Majerle<sup>2</sup>,  
V. S. Pronskikh<sup>1</sup>, A. M. Khilmanovich<sup>4</sup>, B. A. Martsynkevich<sup>4</sup>, I. V. Zhuk<sup>5</sup>,  
V. M. Golovatiouk<sup>1</sup>, W. Westmeier<sup>5</sup>, A. A. Solnyshkin<sup>1</sup>,  
V. M. Tsoupko-Sitnikov<sup>1</sup>, A. S. Potapenko<sup>6</sup>

---

<sup>1</sup>Joint Institute for Nuclear Research, Dubna

<sup>2</sup>Czech Academy of Sciences, Nuclear Physics Institute, Řež near Prague, 250 68  
Czech Republic

<sup>3</sup>HENP Laboratory (ADS Program), Physics Department, University  
of Rajasthan, Jaipur, India

<sup>4</sup>Institute of Physics of National Academy of Sciences, Minsk, Belarus

<sup>5</sup>Kernchemie Institute, Phillips-Universität, Marburg, Germany

<sup>6</sup>Joint Institute of Power and Nuclear Research, Sosny, Minsk, Belarus

<sup>7</sup>University School of Basic and Applied Sciences, GGS IP University,  
New Delhi

\*E-mail: iadam@jinr.ru

Адам И. и др.

E1-2011-52

Изучение скорости реакций  $(n, f)$ ,  $(n, \gamma)$  и  $(n, 2n)$  в  $^{nat}\text{U}$  и  $^{232}\text{Th}$ , производимых потоком нейтронов в графитовой установке (GAMMA-3), облучаемой пучком дейтронов с энергией 2,33 ГэВ

Спалогенные нейтроны, образовавшиеся при взаимодействии пучка дейтронов с энергией 2,33 ГэВ с массивной свинцовой мишенью, тормозятся в толстом графитовом блоке, окружающем мишень, и используются для активации радиоактивных образцов  $^{nat}\text{U}$  и  $^{232}\text{Th}$ , размещенных в трех различных позициях, идентифицируемых как каналы «а», «b» и «с» в графитовом блоке. Скорости реакций  $R(n, f)$ ,  $R(n, \gamma)$  и  $R(n, 2n)$  в обоих образцах определяются с использованием гамма-спектрометрии. Отношения экспериментальных скоростей реакций  $R(n, 2n)/R(n, f)$  для  $^{232}\text{Th}$  и  $^{nat}\text{U}$  оцениваются в целях понимания роли реакций типа  $(n, xn)$  в ADS. Для образцов Th отношение составляет около 54(10)% в случае канала «а» и порядка 95(57)% в случае канала «b» в сравнении с отношением 1,73(20)% для канала «а» и 0,71(9)% в канале «b» для образца  $^{nat}\text{U}$ . Аналогично скорость деления урана по отношению к торию  $^{nat}\text{U}(n, f)/^{232}\text{Th}(n, 2n)$  составляет 11,2(17) в случае канала «а» и 26,8(85) в канале «b». Соответственно, отношение  $^{238}\text{U}(n, 2n)/^{232}\text{Th}(n, 2n)$  равно 0,36(4) для канала «а» и 0,20(10) для канала «b», что указывает на большую вероятность реакции  $(n, xn)$  в  $^{232}\text{Th}$ , чем в  $^{232}\text{U}$ . Все экспериментальные скорости реакций сравнивались с расчетными, полученными при вычислении потоков нейтронов в трех каналах с помощью MCNPX 2.6c и с использованием LA150 — библиотеки поперечных сечений. Экспериментальные и расчетные скорости для всех трех реакций находятся в хорошем согласии. Трансмутационные возможности установки оценивались с использованием скоростей реакций  $(n, \gamma)$  и  $(n, 2n)$  для обоих образцов во всех трех каналах и сравнивались с соответствующими результатами, полученными на установках «Энергия плюс трансмутация» и TARC.

Работа выполнена в Лаборатории ядерных проблем им. В. П. Дзепелова ОИЯИ.

Препринт Объединенного института ядерных исследований. Дубна, 2011

Adam J. et al.

E1-2011-52

A Study of Rates of  $(n, f)$ ,  $(n, \gamma)$ , and  $(n, 2n)$  Reactions in  $^{nat}\text{U}$  and  $^{232}\text{Th}$  Produced by the Neutron Fluence in the Graphite Setup (GAMMA-3) Irradiated by 2.33 GeV Deuteron Beam

Spallation neutrons produced in a collision of 2.33 GeV deuteron beam with the large lead target are moderated by the thick graphite block surrounding the target and used to activate the radioactive samples of  $^{nat}\text{U}$  and Th put at the three different positions, identified as holes «а», «b» and «с» in the graphite block. Rates of the  $(n, f)$ ,  $(n, \gamma)$ , and  $(n, 2n)$  reactions in the two samples are determined using the gamma spectrometry. Ratio of the experimental reaction rates,  $R(n, 2n)/R(n, f)$  for the  $^{232}\text{Th}$  and  $^{nat}\text{U}$  are estimated in order to understand the role of reactions of  $(n, xn)$  type in Accelerator Driven Subcritical Systems. For the Th-sample, the ratio is  $\sim 54(10)\%$  in case of hole «а» and  $\sim 95(57)\%$  in case of hole «b» compared to 1.73(20)% for the hole «а» and 0.710(9)% for the hole «b» in case of the  $^{nat}\text{U}$  sample. Also the ratio of fission rates in uranium to thorium,  $^{nat}\text{U}(n, f)/^{232}\text{Th}(n, f)$ , is  $\sim 11.2(17)$  in case of hole «а» and 26.8(85) in hole «b». Similarly, ratio  $^{238}\text{U}(n, 2n)/^{232}\text{Th}(n, 2n)$  is 0.36(4) for the hole «а» and 0.20(10) for the hole «b» showing that  $^{232}\text{Th}$  is more prone to the  $(n, xn)$  reaction than  $^{238}\text{U}$ . All the experimental reaction rates are compared with the simulated ones by generating neutron fluxes at the three holes from MCNPX 2.6c and making use of LA150 library of cross sections. The experimental and calculated rates of all the three reactions are in good agreement. The transmutation power of the setup is estimated using the rates of  $(n, \gamma)$  and  $(n, 2n)$  reactions for both the samples in the three holes and compared with some of the results of the «Energy plus Transmutation» setup and TARC experiment.

The investigation has been performed at the Dzhelepov Laboratory of Nuclear Problems, JINR.

Preprint of the Joint Institute for Nuclear Research. Dubna, 2011

## 1. INTRODUCTION

Accelerator Driven Subcritical System (ADS) may be identified as a device for i) transmutation of nuclear waste [1, 2] and ii) for production of nuclear energy from the fertile fuel like Thorium [3, 4], besides the safety issues being better than a conventional critical reactor. These two aspects gave birth to new requirement of nuclear data beyond the reactor neutron energies, developing Monte Carlo simulation codes for the design and modeling and developing experiments for the realization of the concept of ADS. It may be recalled that in the existing databases like ENDF, JEFF, JENDL, etc., only few data are available beyond 20 MeV neutron energy. Recently, simulated data up to  $\sim 200$  MeV [5] from the already existing Monte Carlo codes like MCNPX [6], FLUKA [7], and CASCADE [8], deterministic codes like ALICE [9] and TALYS [10] and the parameterization methods after proper evaluation [11] are recently added in the databases. In this direction for getting data on cross sections with better precision in the energy range  $E_n < 20$  MeV and similarly in the energy range of spallation neutrons, a large number of experimental facilities, namely, PNF at Pohang [12], n-ToF at CERN [13], and IREN at Dubna [14], MYRRHA at Belgium [15], SAD [16] and DSAD [17] which later on are identified as «Energy + Transmutation» setup at JINR, etc., were planned and some of them are operational also. Similarly, SINQ at PSI [18], KEK in Japan [19], n-ToF at CERN [13] and a cluster of other research programs are being developed at LANL [20] for obtaining data, characterization and developing new materials. We know that from such facilities at neutron energies beyond 14 MeV, cross sections of a few candidate materials of ADS have also been reported [21] albeit with large errors and much better results are expected to come from 200 meter n-ToF facility at CERN in the near future. In the mean time, for the expeditious realization of the transmutation capability of a system based on the spallation neutrons, a few experiments on transmutation of long-lived fission products like  $^{129}\text{I}$  and  $^{99}\text{Tc}$  by the TARC experiment [22] at CERN and  $^{129}\text{I}$  by the «Energy + Transmutation» (E + T) experiment [23] at JINR, Dubna are conducted and the spectrum averaged transmutation rates are measured. Also, methods of estimation of the transmutation power of a system are developed using the data on fission rates of  $^{232}\text{Th}$  and  $^{nat}\text{U}$ , and the transmutation rates are obtained using the  $(n, \gamma)$  and  $(n, 2n)$  reactions in the neutron field with

the energy ranging from thermal to the beam energy. For obtaining spectrum average reaction rate theoretically, neutron spectrum may be generated from a Monte Carlo simulation code like MCNPX and CASCADE, and point cross sections may be obtained partly from the data bases and partly from deterministic codes like TALYS and ALICE. So, estimated reaction rates are compared with the experimental data. This method is proved to be very useful both for the validation of the Monte Carlo simulation codes [24–28] and for obtaining the spectrum average cross section of a reaction [29].

In the present GAMMA-3 experiment, a huge block of graphite is used to provide a number of positions of moderated spallation neutrons generated by the 2.33 GeV deuteron beam colliding with the lead target where transmutation power of the setup can also be measured using the data of radio-activity corresponding to various gamma peaks of the activated samples almost similarly as in the TARC and E+T experiments. The deuteron beam is used mainly because of technical reason. This experiment differs from the TARC and E+T experiments not only with respect to the beam particle but also having a different moderator. In the TARC experiment a thick lead, in the E+T a natural uranium blanket, and a thick graphite block in the GAMMA-3, are used. The three experiments provide the first data set on the  $(n, \gamma)$ ,  $(n, 2n)$ , and  $(n, f)$  reaction rates at different positions of the setup as well as a comparative study for settling down some of the questions regarding effectiveness of the neutron fluxes at different positions for a given transmutation reaction.

## 2. EXPERIMENTAL DETAILS

In the graphite setup shown in Fig. 1, the lead target of dimensions  $d(\text{dia.}) \times l(\text{length}) = 8 \times 60 \text{ cm}^2$  is placed at the centre of the graphite block of dimensions  $l \times w \times b = 1.1 \times 1.1 \times 0.6 \text{ m}^3$ . The graphite assembly is comprised of 25 blocks of different dimensions having several experimental holes for placing the activation samples and detectors.  $^{232}\text{Th}$  sample is placed in three holes marked as «a», «b» and «c» in the blocks number 14, 9, and 4, respectively, as shown in Fig. 1. The dimensions of the holes «a», «b» and «c» are  $d \times l = 14.6 \times 29.6 \text{ cm}^2$ ,  $8.8 \times 36.3 \text{ cm}^2$ ,  $15.4 \times 34.1 \text{ cm}^2$ , respectively. Samples of  $^{\text{nat}}\text{U}$  are placed in two holes, «a» and «b» while samples of  $^{232}\text{Th}$  are placed in all the three holes. Blocks number 3, 4, and 5 and several other blocks visible in Fig. 1 are used for other transmutation samples accompanied by threshold activation detectors. Uranium and thorium samples were irradiated in the form of sandwiches of three nearly identical foils (Th-Th-Th and U-U-U). This arrangement has a little advantage compared to a single foil that some of the nuclides produced in the sideward foils may be registered in adjoining foil. We used single (middle) foil and the double (sideward) foils for separate measurements because of the difference in

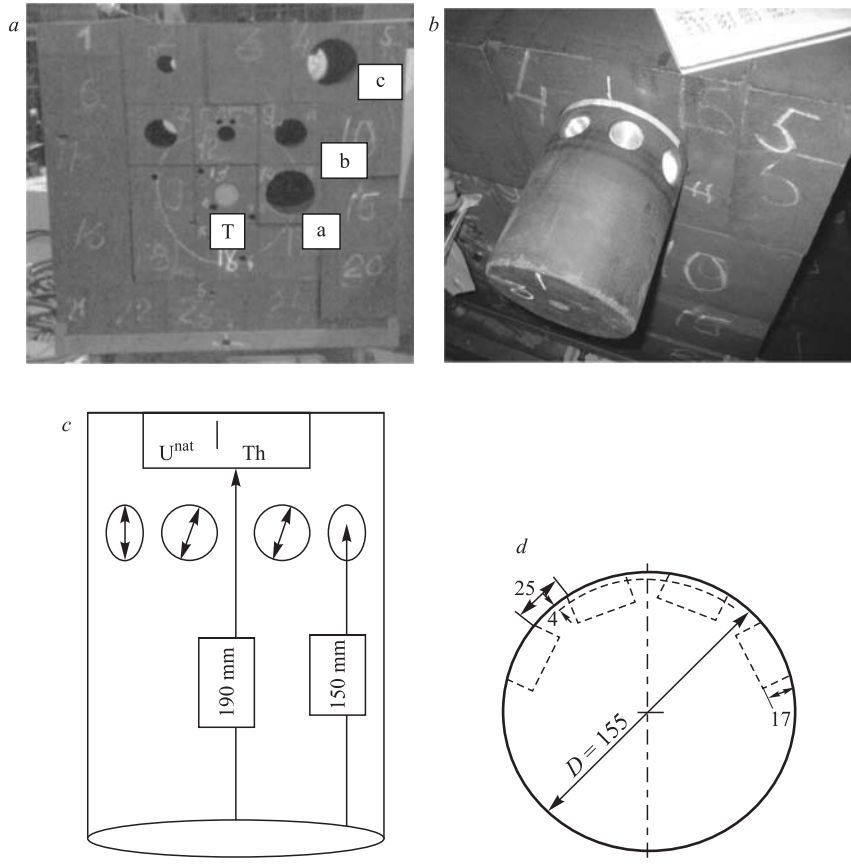


Fig. 1. Graphite assembly (a) of dimensions  $1.1 \times 1.1 \times 0.6 \text{ m}^3$  with the lead target, T of diameter 8 cm at the centre and three experimental holes shown as «a», «b» and «c» for the irradiation of different samples. Photograph of the fitted cylinder (b) in a hole is shown for the clarity. The sample positions inside a hole are shown in (c) as well they are seen in the photograph also. The positions of the samples on the cylinder fitted in a hole are shown in (d).  $^{nat}\text{U}$  and  $^{232}\text{Th}$  are placed at  $-9^\circ$  and  $+9^\circ$  in hole «a», at  $-14^\circ$  and  $+14^\circ$  in hole «b» and at  $-9^\circ$  and  $+9^\circ$  in hole «c», respectively, from the centre of the front face of the respective cylinder to the back of the circles. Four circles shown on the cylindrical surface are for other samples placed in the experiment

self-absorption of the low-energy gamma rays being much higher compared to that of high-energy gammas (see Fig. 3). Use of single layer is preferred for the analysis of low-energy gammas and for the high-energy gammas double layered foils are used. Also, it provides improved statistics.

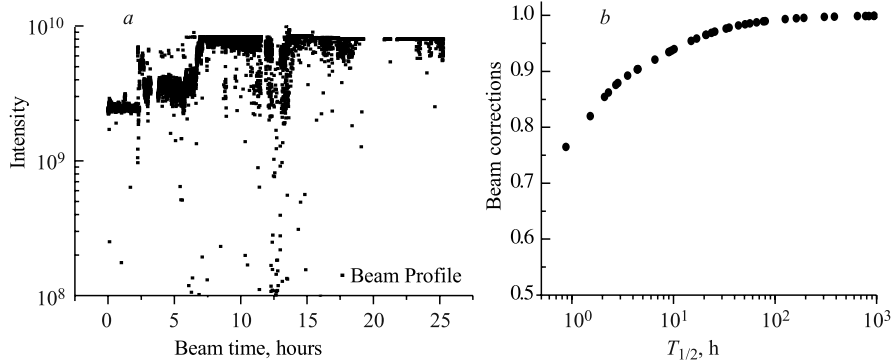


Fig. 2. (a) Time dependence of the 2.33 GeV deuteron beam intensity (the number of deuterons per one pulse), as received from the staff of the Nuclotron accelerator for the whole run. (b) Beam corrections for residual nuclei in increasing order of  $\eta_b$  of elements:  $^{134}\text{I}$ ,  $^{133}\text{Te}$ ,  $^{142}\text{La}$ ,  $^{127}\text{Sn}$ ,  $^{132}\text{I}$ ,  $^{92}\text{Sr}$ ,  $^{88}\text{Kr}$ ,  $^{92}\text{Y}$ ,  $^{129}\text{Sb}$ ,  $^{105}\text{Ru}$ ,  $^{135}\text{Xe}$ ,  $^{128}\text{Sb}$ ,  $^{140}\text{Ba}$ ,  $^{93}\text{Y}$ ,  $^{91}\text{Sr}$ ,  $^{24}\text{Na}$ ,  $^{97}\text{Zr}$ ,  $^{133}\text{I}$ ,  $^{112}\text{Pd}$ ,  $^{187}\text{W}$ ,  $^{143}\text{Ce}$ ,  $^{105}\text{Ru}$ ,  $^{48}\text{Sc}$ ,  $^{238}\text{Np}$ ,  $^{99}\text{Mo}$ ,  $^{132}\text{Te}$ ,  $^{47}\text{Sc}$ ,  $^{131}\text{I}$ ,  $^{48}\text{Sc}$ ,  $^{95}\text{Nb}$ , and  $^{103}\text{Ru}$  nuclides

Diameter of these foils is 15 mm and mass of the middle U foil is 172.3 mg, the mass of the middle  $^{232}\text{Th}$  foil is 93.1 mg while the total mass of the sideward foils is 334 mg for U and 176.3 mg for  $^{232}\text{Th}$ .

The setup was irradiated by the deuteron beam of 2.33 GeV energy at the Nuclotron accelerator in Dubna in March, 2007. The irradiation started at 13 : 44 : 25 h on March 17, 2007 and ended at 15 : 01 : 20 h on March 18, 2007, i.e., it lasted for about 25 hours and 17 minutes (= 1517 minutes). The recorded intensity profile of the beam versus time is shown in Fig. 2, a. From the given time dependence of the beam, a correction  $\eta_b(T_{1/2})$  is calculated for each residual reaction product with the half-life  $T_{1/2}$  and is displayed in Fig. 2, b. Activation detectors, solid state nuclear track detectors and transmutation samples are used to measure the spectral fluences of the neutron field.

An aluminum foil (with thickness  $6.7 \text{ mg/cm}^2$  and diameter 20 cm each) was installed at a distance of 3.1 m from the centre of the lead target in order to determine the beam profile and the number of deuterons hitting the lead target. The deuterons have been monitored using the reaction  $^{27}\text{Al}(d, 3p 2n)^{24}\text{Na}$  [30] through the gamma spectrometry of the product nuclide  $^{24}\text{Na}$ . After irradiation, the monitor foil was cut into four concentric rings with the inner ring having a circle of 2.1 cm in diameter, the three following rings having outer diameters as 8.0, 12.0, and 16.0 cm, respectively. The number of deuterons measured on the two inner rings up to 8 cm diameter was 92(4)% of the total beam, and the integral number of deuterons hitting the Pb target is deduced to be

$N_d = (1.70 \pm 0.10) \cdot 10^{13}$ . From the track detectors the beam shape (see [23]) is established to be Gaussian with parameters,  $X(\text{FWHM}) = 1.5 \pm 0.1$  cm,  $Y(\text{FWHM}) = 2.4 \pm 0.1$  cm and of the beam center being at  $X_c = 0.7 \pm 0.1$  cm,  $Y_c = 0.2 \pm 0.1$  cm. From the track detectors the integral number of deuterons comes out to be  $\sim 1.85 \cdot 10^{13}$  and the percentage of beam hitting the lead to be 92.2% which agrees with the data obtained from the Al monitor.

### 3. MEASUREMENT PROCEDURE AND METHOD OF ANALYSIS

We have used the coaxial detector with relative efficiency of 18.9% and resolution being 1.78 keV at 1332 keV and a planar detector with diameter 36 mm, thickness 13 mm and resolution 335 eV at 5.9 keV and 580 eV at 122 keV. Coaxial detector is used to provide information on peaks ranging from 20 keV to 3 MeV and a planar detector is used for  $\sim 5$  keV to 700 keV.

All measurements have been done without any filters. Various measurement spectra are recorded up to a period of about one month for the time intervals varying between 0.4 to 24 hours.

Measured gamma spectra are analyzed by interactive mode of the DEIMOS code [31]. A detailed cascade of codes has been used for the energy calibration, subtraction of background gamma-ray lines and single and double escape peaks, efficiency calibration and determination of experimental half-lives for the identification of several hundreds of gamma-ray lines. Various isotopes and fission fragments are assigned only when energy, half-life, and intensity of peaks match

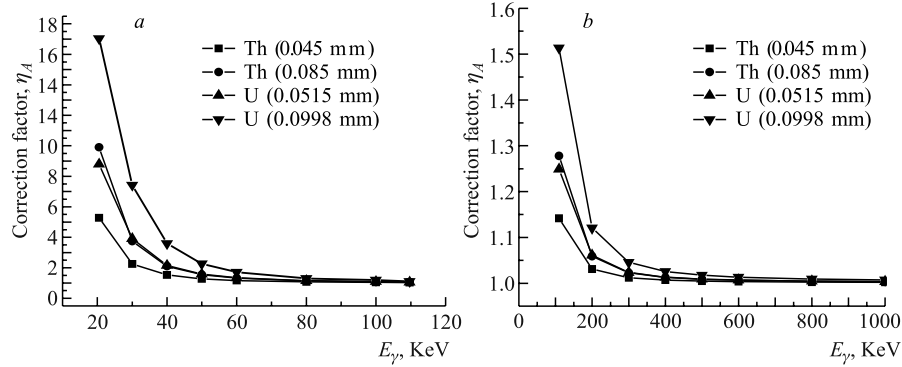


Fig. 3. Self-absorption correction factor,  $\eta_A$ , for single and double thicknesses of  $^{232}\text{Th}$  and  $^{\text{nat}}\text{U}$  samples for the gamma energy range *a*) low (for Th from 20.47 to 109.65 keV and for U from 21.76 to 115.61 keV), *b*) high (for Th from 109.65 to 1000 keV and for U from 115.61 to 1000 keV)

with the values available in the literature [32]. For the details of the method of analysis of gamma peaks reader is addressed to [23].

After identification and assignment of the element to a gamma peak the reaction rates have been calculated for every identified element with all the relevant correction factors of self-absorption  $\eta_a$ , beam intensity fluctuations  $\eta_b$ , and coincidence summing  $\eta_c$  (see appendix in [23]). Values of  $\eta_a$ ,  $\eta_b$ ,  $\eta_c$  have been estimated for the gamma peaks separately for the two samples of  $^{232}\text{Th}$  and  $^{\text{nat}}\text{U}$ . Self-absorption correction,  $\eta_a$ , for the two sideward double and middle single layers of the  $^{232}\text{Th}$  and  $^{\text{nat}}\text{U}$  samples are plotted in Figs. 3, *a, b* for the low- and high-energy gammas, respectively, and from both the figures it can be seen clearly that for low-energy gammas  $\eta_a$  is very high while for the high energies it is close to unity. At energies beyond 1000 keV correction is less than 1% and is monotonously decreasing to zero with the increasing of energy.

The coincidence summing correction,  $\eta_c$  is calculated using the software COICOR and the Lund database [32], and this correction depends also on the total efficiency of registration of gamma rays including the Compton scattering tail. The total correction factor,  $\eta = \eta_a \eta_b \eta_c$  is given for each observed peak in Tables 1 and 2.

The reaction rate,  $R(A_r, Z_r)$  is defined as the number of produced residual nuclei,  $Q(A_r, Z_r)$  per atom ( $N_t$ ) of the sample per incident beam deuteron per second ( $N_d$ ) as follows:

$$R(A_r, Z_r) = \frac{Q(A_r, Z_r)}{N_t N_d}. \quad (1)$$

The transmutation power,  $P(A_r, Z_r)$  is defined as the quantity of produced mass  $m(A_r, Z_r)$  per unit mass of the target  $m(A_t, Z_t)$  [23], and on normalization to  $10^9$  beam particles we can write,

$$P_{\text{norm}}(A_r, Z_r) = 10^9 \frac{P(A_r, Z_r)}{N_D}, \quad (2)$$

where  $N_D$  is the integral number of beam particles used in the irradiation time,  $t_{\text{irr}}$ .

#### 4. EXPERIMENTAL RESULTS OF REACTION RATES

After following all the detailed procedure related to the gamma spectrometry technique [23], the results in term of reaction rate,  $R$  of the measurement of  $\gamma$ -rays from both the samples of  $^{232}\text{Th}$  in the three irradiation holes «a», «b» and «c» are given in Table 1. Table 2 corresponds to the results of  $^{\text{nat}}\text{U}$  of holes «a» and «b». All the observed fission fragments and residual nuclides are listed

Table 1. Results of activity [Bq], half-life,  $T_{1/2}$ , average reaction rate,  $\langle R \rangle$  for the  $^{232}\text{Th}$  after irradiation by secondary neutrons in the holes «a», «b» and «c». All corrections are included in  $\eta$ . (\*) denotes mixing due to other nuclide. Letters «M» correspond to number of  $\gamma$ -ray spectra, «X» to planar and «C» to coaxial detectors and «s» and «d» to the single and double layers of the sample, respectively

Isotope $E_\gamma$ [keV]	Activity [Bq] $I_\gamma$ [%]	$\eta$ -XsM $\eta$ -CdM	a hole		b hole		c hole	
			$T_{1/2}$ (Lib.) $T_{1/2}$ (Exp.)	$\langle R \rangle$ R	$T_{1/2}$ (Lib.) $T_{1/2}$ (Exp.)	$\langle R \rangle$ R	$T_{1/2}$ (Lib.) $T_{1/2}$ (Exp.)	$\langle R \rangle$ R
<b>Th-231</b>	<b>371(37)</b>		<b>25.52(10) h</b>	<b>(7.61(83)E-27)</b>	<b>25.52(10) h</b>	<b>(3.6 (18)E-27)</b>		
25.646	14.50	3.900-Xs5	23.4(26) h	1.49(91)E-26	7.47h	3.41(97)E-27	Xs2	
25.646	14.50	5.337-Xd4	25.44(14)h	1.43(93)E-26				
81.227	0.89	1.107-Xs5	5.0(9)d	8.9(18)E-27	13(4)d	3.6(18)E-27	Xs7	
81.227	0.89	1.192-Xd5	6.5(18)d	8.6(26)E-27				
84.216	6.60	1.037-Xs7	12(3)d	6.5(11)E-27	—	4.9(21)E-27	Xs7	
84.216	6.60	1.105-Xd6	18(9)d	8.9(25)E-27				
89.944	0.94	1.070-Xs7	—	1.63(25)E-25*				
89.944	0.94	1.121-Xd6	87(25)d	2.04(6)E-25*				
<b>Pa-233</b>	<b>419(11)</b>		<b>26.967(2) d</b>	<b>(3.20(8)E-25)</b>	<b>26.967(2) d</b>	<b>(1.92(5)E-25)</b>		<b>(3.38(16)E-26)</b>
75.354	1.39	1.189-Xs7	160(80)d	3.7(20)E-25	—	2.39(26)E-25	Xs7	1.31(21)E-25*
75.354	1.39	1.222-Xd6	—	5.5(16)E-25	100(40)d	2.49(32)E-25	Xd6	1.19(9)E-25*
86.814	1.97	1.096-Xs7	33(19)d	6.0(33)E-25	67(17)d	4.6(17)E-25*	Xs7	2.81(12)E-25*
86.814	1.97	1.172-Xd6	58(9)d	7.2(27)E-25	49(7)d	4.7(19)E-25*	Xd6	3.48(15)E-25*
103.941	0.87	1.108-Xs6	42(11)d	3.46(77)E-25	20(4)d	1.94(8)E-25	Xs7	4.70(58)E-25*
103.941	0.87	1.122-Xd6	31(3)d	3.9(12)E-25	26(3)d	2.25(8)E-25	Xd6	5.8(12)E-25*
103.941	0.87	1.124-Cd2	—	3.81(77)E-25				
300.110	6.62	1.016-Xs7	42(4)d	4.1(12)E-25	49(8)d	2.86(9)E-25*	Xs7	1.36(5)E-25*
300.110	6.62	1.027-Xd6	41.8(28)d	5.1(12)E-25	54(10)d	3.13(21)E-25*	Xd6	1.59(12)E-25*
300.110	6.62	1.025-Cd3	38.8(12)d	5.4(24)E-25	39(11)d	3.28(13)E-25*	Cd4	1.70(15)E-25*
311.890	38.6	1.021-Xs7	29.2(2)d	2.78(7)E-25	30(4)d	1.69(4)E-25	Xs7	3.04(9)E-26
311.890	38.6	1.031-Xd6	28.9(9)d	3.48(9)E-25	29(3)d	1.83(9)E-25	Xd6	3.46(23)E-26
311.890	38.6	1.026-Cd3	25.9(6)d	3.66(14)E-25	20.6(18)d	1.99(7)E-25	Cd4	3.79(13)E-26
340.710	4.47	1.012-Xs7	36(9)d	2.95(8)E-25	19(9)d	1.83(7)E-25	Xs7	4.7(27)E-26

Table 1. Continuation

Isotope $E_{\gamma}$ [keV]	Activity [Bq]	$\eta$ -XsM $\eta$ -CdM	a hole		b hole		c hole			
			$T_{1/2}$ (Lib.) $T_{1/2}$ (Exp.)	$\langle R \rangle$ R	$T_{1/2}$ (Lib.) $T_{1/2}$ (Exp.)	$\langle R \rangle$ R	$T_{1/2}$ (Lib.) $T_{1/2}$ (Exp.)	$\langle R \rangle$ R		
340.710	4.47	1.020-Xd6	21.9(18)d	3.78(11)E-25	36(11)d	2.05(15)E-25	Xd6	44(11)d	5.7(24)E-26	Xd6
340.710	4.47	1.019-Cd3	31(4)d	3.87(20)E-25	25(3)d	2.16(9)E-25	Cd4	47(9)d	5.8(35)E-26	Cd3
375.450	0.679	0.981-Xs3	23(14)d	3.01(20)E-25	13(7)d	2.16(20)E-25	Xs3			
375.450	0.679	0.986-Xd6	33(9)d	3.8(19)E-25	17(5)d	2.23(24)E-25	Xd5			
375.450	0.679	0.984-Cd3	27(4)d	4.3(16)E-25	29(12)d	2.75(17)E-25	Cd3			
398.620	1.390	0.929-Xs6	24(8)d	3.1(13)E-25	—	1.87(15)E-25	Xs4			
398.620	1.390	0.932-Xd6	37(10)d	3.8(14)E-25	17(5)d	2.22(12)E-25	Xd3			
398.620	1.390	0.927-Cd3	25.3(11)d	3.9(14)E-25	37(4)d	2.02(7)E-25	Cd4			
415.760	1.745	0.970-Xs6	26(8)d	2.8(11)E-25	18(4)d	1.85(8)E-25	Xs5	6.93(0.07)d	6.3(12)E-26	Xs2
415.760	1.745	0.975-Xd6	27(5)d	3.5(12)E-25	—	1.94(8)E-25	Xd4	11.3(0.01)d	5.29(74)E-26	Xd2
415.760	1.745	0.973-Cd3	28.4(2)d	3.9(16)E-25	20.6(2.8)d	2.13(7)E-25	Cd4	—	5.21(62)E-26	Cd2
<b>Kr-85m</b>	<b>5.57(6)</b>		<b>4.48(8)h</b>	<b>(3.15(4)E-29)</b>	<b>4.48(8)h</b>	<b>(7.25(85)E-30)</b>				
151.159	75	1.017-Xs4	1.7(9)d	3.16(6)E-29	—	7.4(12)E-30	Xs1			
151.159	75	1.130-Xd2	9.57(1)h	3.15(5)E-29						
<b>Mo-99</b>	<b>2.37(19)</b>		<b>2.748(4)d</b>	<b>(1.99(19)E-28)</b>	<b>2.748(4) d</b>	<b>(5.55(88)E-29)</b>			<b>(5.5(19)E-30)</b>	
140.681	89.43	1.023-Xs7	4.6(4)d	2.13(13)E-28	—	5.55(88)E-29	Xs3	—	5.5(19)E-30	Xs1
140.681	89.43	1.137-Xd4	11(4)d	1.75(12)E-28						
140.681	89.43	1.135-Cd2		2.56(26)E-28						
<b>I-131</b>	<b>0.70(24)</b>		<b>8.021d</b>	<b>(1.69(59)E-28)</b>	<b>8.021d</b>	<b>(1.39(54)E-28)</b>				
364.489	81.7	1.047-Xs1	—	1.66(81)E-28	—					
364.489	81.7	1.027-Xd1		1.73(85)E-28		1.39(54)E-28	Xd1			
<b>Xe-133</b>	<b>1.89(12)</b>		<b>5.243(1)d</b>	<b>(3.00(20)E-28)</b>						
80.997	38	1.062-Xs3	1.5(6)d	3.32(13)E-28						
80.997	38	1.263-Xd4	3.5(17)d	2.88(8)E-28						
<b>Xe-135</b>	<b>12.6(13)</b>		<b>9.14(02)h</b>	<b>(1.06(14)E-28)</b>						
249.770	90	0.969-Xs4	16.1(25)h	1.02(13)E-28						
249.770	90	1.000-Xd3	12.1(11)h	1.52(43)E-28						
<b>Ce-141</b>	<b>0.26(2)</b>		<b>32.50(5)d</b>	<b>(2.52(74)E-28)</b>	<b>32.50(5)d</b>	<b>(6.6(29)E-29)</b>				

Table 1. Continuation

Isotope $E_\gamma$ [keV]	Activity [Bq] $I_\gamma$ [%]	a hole		b hole		c hole	
		$T_{1/2}$ (Lib.) $T_{1/2}$ (Exp.)	$\langle R \rangle$ R	$T_{1/2}$ (Lib.) $T_{1/2}$ (Exp.)	$\langle R \rangle$ R	$T_{1/2}$ (Lib.) $T_{1/2}$ (Exp.)	$\langle R \rangle$ R
145.441	48.2	1.136-Xs1	2.8(12)E-28	—	6.6(29)E-29	Xs1	
145.441	48.2	1.275-Xd2	7.74(8)d				

Note: Averaging is done without including the data marked with sign (\*). Activities are calculated for Th sample having mass 0.0932 g and assuming the start of measurement time to be the end of irradiation.

Table 2. Results of activity [Bq], half-life,  $T_{1/2}$ , average reaction rate,  $\langle R \rangle$  for the  $^{238}\text{U}$  after irradiation by secondary neutrons in the holes «a» and «b». All corrections are included in  $\eta$ . (\*) denotes mixing due to other nuclide. Letters «M» correspond to number of  $\gamma$ -ray spectra, «X» to planar and «C» to coaxial detectors and «s» and «d» to the single and double layers of the sample, respectively

Isotope $E_\gamma$ [keV]	Activity [Bq] $I_\gamma$ [%]	$\eta$ -XsM $\eta$ -CdM	a hole		b hole	
			$T_{1/2}$ (Lib.) $T_{1/2}$ (Exp.)	$\langle R \rangle$ R	$T_{1/2}$ (Lib.) $T_{1/2}$ (Exp.)	$\langle R \rangle$ R
U-237	22.8(8)		6.75 (1)d	(2.72(9)E-27)	6.75 (1) d	(7.21(20)E-28)
26.345	2.43	11.67-Xd2	18.27d	7.3(13)E-26*		
26.345	2.43	6.374-Xs2	16d	1.89(50)E-26*		
59.541	34.5	1.821-Xd6	7.5(3)d	2.70(10)E-27	—	7.37(10)E-28 Xd2
59.541	34.5	1.413-Xs7	8.3(5)d	2.85(15)E-27	16.6h	6.95(13)E-28 Xs2
208.00	21.2	1.199-Xd6	6.7(4)d	2.52(10)E-27		
208.00	21.2	1.139-Xs7	7.1(5)d	2.97(12)E-27		
208.00	21.2	1.560-Cd3	5.7(5)d	1.64(75)E-27		
Np-239	7200(240)		2.3565(4) d	(3.11(10)E-25)	2.3565(4) d	(2.08(20)E-25)
44.665	0.13	3.130-Xd4	2.6(3)d	3.66(27)E-25	1.91(21)d	2.70(56)E-25 Xd6
44.665	0.13	2.023-Xs4	3.0(4)d	2.65(22)E-25	1.3(6)d	3.74(75)E-25 Xs3
49.415	0.13	2.674-Xd7	5.0(6)d	8.7(22)E-25*	7.5(12)d	6.08(55)E-25* Xd6

Table 2. Continuation

Isotope $E_\gamma$ [keV]	Activity [Bq]	$I_\gamma$ [%]	$\eta$ -XsM $\eta$ -CdM	a hole		b hole		XsM CdM
				$T_{1/2}$ (Lib.) $T_{1/2}$ (Exp.)	$\langle R \rangle$ R	$T_{1/2}$ (Lib.) $T_{1/2}$ (Exp.)	$\langle R \rangle$ R	
49.415	0.13		1.968-Xs7	4.21(29)d	7.1(15)E-25*	5.0(4)d	7.9(34)E-25*	Xs7
57.276	0.13		2.184-Xd6	1.65(5)d	7.6(16)E-25*	1.49(10)d	6.2(23)E-25*	Xd6
57.276	0.13		1.651-Xs7	1.78(8)d	8.3(11)E-25*	1.6(1)d	4.8(25)E-25*	Xs5
61.461	1.29		1.690-Xd6	2.28(5)d	3.61(12)E-25	2.44(2)d	1.90(63)E-25	Xd6
61.461	1.29		1.350-Xs7	2.47(3)d	2.95(10)E-25	2.36(5)d	2.67(75)E-25	Xs6
61.461	1.29		1.764-Cd3	2.26(6)d	2.77(21)E-25			
67.846	0.092		1.809-Xd6	2.29(11)d	5.9(7) E-25	3.21(1)d	2.71(47)E-25	Xd6
67.846	0.092		1.433-Xs7	2.39(18)d	3.89(40)E-25	2.7(5)d	3.24(63)E-25	Xs3
106.125	27.2		1.117-Xs7	2.40(11) d	2.94(7)E-25	2.368(27) d	1.86(5)E-25	Xs6
106.125	27.2		1.184-Xd6	2.35(6) d	3.75(10)E-25	2.41(03) d	2.02(6)E-25	Xd6
106.125	27.2		1.172-Cd3	2.34(2) d	3.04(14)E-25	3.71(15) d	1.99(3)E-25	Cd3
181.711	0.081		1.181-Xd4	1.81(20)d	3.33(31)E-25			
181.711	0.081		1.085-Xs5	2.5(3)d	2.74(23)E-25			
209.753	3.42		1.092-Xs7	2.39(12) d	3.97(9)E-25	2.38(4) d	3.18(6)E-25	Xs6
209.753	3.42		1.174-Xd6	2.32(4) d	4.91(12)E-25	2.41(19) d	3.59(12)E-25	Xd6
209.753	3.42		1.135-Cd4	2.43(3) d	4.69(28)E-25	2.20(5) d	2.88(19)E-25	Cd4
226.378	0.28		1.113-Xd6	2.25(12)d	3.53(19)E-25	2.11(19)d	5.06(83)E-25	Xs5
226.378	0.28		1.069-Xs7	2.40(9)d	2.99(16)E-25	3.1(4)d	2.12(47)E-25	Xd6
228.183	10.76		1.087-Xs7	2.48(9) d	3.62(9)E-25*	—	2.14(5)E-25*	Xs2
228.183	10.76		1.152-Xd6	2.41(4) d	4.53(15)E-25*	2.53(18) d	3.01(8)E-25*	Xd6
228.183	10.76		1.082-Cd4	2.46(6) d	4.14(12)E-25*	2.10(3) d	2.69(32)E-25*	Cd4
254.418	0.11		1.072-Xd5	1.98(19) d	3.63(37)E-25	—	1.92(35)E-25	Xd6
254.418	0.11		1.039-Xs5	1.35(13)d	3.21(50)E-25	1.6d	2.26(59)E-25	Cd2
254.418	0.11		1.085-Cd1		2.56(4)E-25			
277.599	14.38		1.075-Xs7	2.38(15) d	3.16(7)E-25	2.32(23) d	1.88(35)E-25	Xs6
277.599	14.38		1.115-Xd6	2.35(30) d	3.98(10)E-25	2.39(4) d	1.84(28)E-25	Xd6
277.599	14.38		1.079-Cd4	2.34(19) d	3.38(13)E-25	2.5(6) d	2.15(29)E-25	Cd4
285.460	0.79		1.107-Xd5	2.26(6) d	2.48(22)E-25	2.42(8)d	1.81(34)E-25	Xd6

Table 2. Continuation

Isotope $E_\gamma$ [keV]	Activity [Bq]	$\eta$ -XsM $\eta$ -CdM	a hole		b hole		XsM CdM
			$T_{1/2}$ (Lib.) $T_{1/2}$ (Exp.)	$\langle R \rangle$ R	$T_{1/2}$ (Lib.) $T_{1/2}$ (Exp.)	$\langle R \rangle$ R	
285.460	0.79	1.080-Xs7	2.44(6)d	2.78(9)E-25	1.53d	1.66(21)E-25	Xs2
285.460	0.79	1.135-Cd1		3.61(16)E-25	3.0(17)d	2.53(79)E-25	Cd3
315.879	1.60	0.923-Xs7	2.34 (3) d	2.95(9)E-25	2.35(8) d	1.89(15)E-25	Xs6
315.879	1.60	0.941-Xd6	2. 32(4) d	3.73(22)E-25	2.34(4)d	1.72(6)E-25	Xd5
315.879	1.60	0.946-Cd3	2.34(16) d	2.34(16)E-25	2.34(16)d	2.07(4)E-25	Cd3
334.309	2.07	0.828-Xs7	2.47(4) d	2.99(10)E-25	2.37(08) d	1.98(13)E-25	Xs7
334.309	2.07	0.842-Xd6	2.32(5) d	3.65(22)E-25	2.47(7) d	1.67(6)E-25	Xd5
334.309	2.07	0.848-Cd4	2.34(3) d	3.29(13)E-25	3.1(2) d	2.13(5)E-25	Cd3
<b>Kr-85m</b>	<b>126(5)</b>		<b>4.480(8)h</b>	<b>(1.58(6)E-27)</b>	<b>4.480(8)h</b>	<b>(9.05(18)E-29)</b>	
151.159	75	1.130-Xd2	4.4h	1.63(8)E-27	4.49h	1.14(8)E-28	Xd2
151.159	75	1.017-Xs4	4.65(13)h	1.52(7)E-27	3.9(5)h	9.04(55)E-29	Xs3
304.870	75	0.923-Xs3	3.8(19)h	2.09(37)E-27			
<b>Y-93</b>	<b>374(18)</b>		<b>10.18(8)h</b>	<b>(5.60(27)E-27)</b>			
266.90	7.3	1.011-Xd3	11.0(9) h	5.82(43)E-27			
266.90	7.3	1.002-Xs4	10.5(9)h	5.47(33)E-27			
<b>Zr-97</b>	<b>638(149)</b>		<b>16.74(11)h</b>	<b>(7.5(17)E-27)</b>	<b>16.744(11h)</b>	<b>(4.69(33)E-27)</b>	
743.36	93	0.964-Cd3	18(10)h	7.5(17)E-27	12(8)d	4.69(33)E-27	Cd3
<b>Mo-99</b>	<b>129(3)</b>		<b>2.7475(4) d</b>	<b>(6.76(18) E-27)</b>	<b>2.7475(4) d</b>	<b>(3.53(46)E-27)</b>	
140.681	89.43	1.081-Xs7	2.845(24) d	6.47(40)E-27	2.94(12) d	3.21(91)E-27	Xs7
140.681	89.43	1.291-Xd6	2.80(8) d	6.90(26)E-27	2.98(5) d	5.2(15)E-27	Xd5
140.681	89.43	1.292-Cd4	3.06(09) d	8.2(21)E-27	2.90(6) d	6.1(24)E-27	Cd4
181.063	5.99	1.092-Xs6	4.0(12) d	7.0(6)E-27	2.1(5) d	2.87(20)E-27	Xs4
181.063	5.99	Xd5	3.23(21) d	6.74(44)E-27			
739.500	12.13	1.108-Cd4	3.1(7) d	5.52(99)E-27	3.3(2) d	4.77(28)E-27	Cd4
<b>Ru-103</b>	<b>5.0(3)</b>		<b>39.26(20)d</b>	<b>(3.41(12) E-27)</b>	<b>39.26(20)d</b>	<b>(2.60(37)E-27)</b>	
497.080	90.9	1.017-Xd3	27(20) d	3.40(33)E-27	—	3.21(75)E-27	Xd1
497.080	90.9	1.016-Xs3	80(70) d	3.49(27)E-27	28(20)d	2.40(43)E-27	Cd4
497.080	90.9	1.017-Cd3	39(4)d	3.39(14)E-27			

Table 2. Continuation

Isotope $E_\gamma$ [keV]	Activity [Bq]	$I_\gamma$ [%]	$\eta$ -XsM $\eta$ -CdM	a hole		b hole		XsM CdM
				$T_{1/2}$ (Lib.) $T_{1/2}$ (Exp.)	$\langle R \rangle$ R	$T_{1/2}$ (Lib.) $T_{1/2}$ (Exp.)	$\langle R \rangle$ R	
<b>Rh-105</b>	<b>106(9)</b>			<b>35.36(60)h</b>	<b>(1.40(9)E-27)</b>	<b>35.36 (6)h</b>	<b>(8.2(9)E-28)</b>	
319.14	19		1.031-Xd4	65(10) h	1.35(13) E-27	—	9.2(17)E-28	Xd1
319.14	19		1.022-Xs4	34.6(55) h	1.45(13)E-27	—	7.8(11)E-28	Cd1
<b>I-131</b>	<b>21.2(5)</b>			<b>8.021(11)d</b>	<b>(3.02(6)E-27)</b>	<b>8.021(11) d</b>	<b>(2.26(31)E-27)</b>	
284.305	6.14		1.046-Xd2	9.3 d	3.9(6)E-27	2.42(8)d	2.29(67)E-27	Xd5
284.305	6.14		1.022-Xs1	—	3.8(10)E-27	—	—	
364.489	81.7		1.047-Xd6	8.6(3) d	2.97(9)E-27	9.2(6)d	1.95(52)E-27	Xd6
364.489	81.7		1.031-Xs6	7.8(7) d	2.99(13)E-27	10.0(14)d	3.08(83)E-27	Xs5
364.489	81.7		1.047-Cd4	8.14(13)d	3.07(11)E-27	6.4(17)d	2.24(59)E-27	Cd4
<b>Te-132</b>	<b>71(20)</b>			<b>3.204(2) d</b>	<b>(3.42(19)E-27)</b>	<b>3.204(2) d</b>	<b>(3.45(12)E-27)</b>	
49.720	15.0		2.486-Xd6	5.0(6)d	1.01(47)E-26*	—	1.27(7)E-26*	Xd6
49.720	15.0		-Xs7	4.21(29) d	7.59(77)E-27*	—	—	
228.160	88.0		1.041-Xs7	2.49(9) d	3.41(47)E-26*	—	—	
228.160	88.0		1.094-Xd6	2.49(4) d	3.2(6)E-26*	2.53(18) d	3.00(9)E-26*	Xd6
228.160	88.0		1.085-Cd4	2.46(6) d	3.9(14)E-26*	2.10(3) d	2.53(6)E-26*	Cd4
522.650	16.6		1.154-Xs3	5.1(28) d	5.09(43)E-27	—	—	
522.650	16.6		1.167-Xd4	3.4(9) d	4.27(33)E-27	—	3.32(5)E-27	Xd6
522.650	16.6		1.286-Cd2	2.91(29) d	4.19(28)E-27	—	3.52(22)E-27	Cd2
630.190	13.3		1.096-Xd6	4.9(2)d	2.94(8)E-27	—	—	
630.190	13.3		1.154-Cd3	4.9(2)d	2.99(11)E-27	—	3.87(8)E-27	Cd2
667.72	101.7		1.084-Xs7	3.11(14) d	4.21(15)E-27	—	—	
667.72	101.7		1.089-Xd5	3.42(15) d	4.22(16)E-27	—	—	
667.72	101.7		1.159-Cd3	3.07(5) d	3.49(15)E-27	3.3(1) d	2.69(38)E-27	Cd3
772.61	77.9		0.994-Cd3	3.05(8) d	3.55(16)E-27	3.7(2) d	2.80(37)E-27	Cd3
954.55	18.7		0.993-Cd3	5.0(11) d	3.91(26)E-27	3.8(1) d	3.09(27)E-27	Cd3
<b>I-133</b>	<b>302(7)</b>			<b>20.8(1) h</b>	<b>(6.40(27)E-27)</b>	<b>20.8(1) h</b>	<b>(3.35(15)E-27)</b>	
529.87	86.3		0.969-Xs5	20.8(7) h	6.35(22)E-27	—	3.28(5)E-27	Xs2
529.87	86.3		0.980-Xd4	21.0(7) h	6.69(22)E-27	21.7 h	3.10(13)E-27	Xd4

Table 2. Continuation

Isotope $E_\gamma$ [keV]	Activity [Bq]	$\eta$ -XsM $\eta$ -CdM	a hole		b hole		XsM CdM
			$T_{1/2}$ (Lib.) $T_{1/2}$ (Exp.)	$\langle R \rangle$ R	$T_{1/2}$ (Lib.) $T_{1/2}$ (Exp.)	$\langle R \rangle$ R	
529.87	86.3	0.980-Cd4	22.68 h	5.31(48)E-27	30.96 h	3.84(11)E-27	Cd3
<b>Xe-133</b>	<b>141(21)</b>		<b>5.243(1) d</b>	<b>(1.25(18)E-26*)</b>	<b>5.243(1)d</b>	<b>(3.97)E-27</b>	
80.997	38	1.620-Xd6	7.8(5) d	1.33(9)E-26*	—	3.6(10)E-27	Xd6
80.997	38	1.301-Xs7	13.3(24) d	8.7(19)E-27*	7.4(12)d	4.1(10)E-27	Xs7
160.613	0.066	0.994-Xd2		1.16(36)E-25*			
160.613	0.066	0.912-Xs6	4.0(12)d	1.33(18)E-25*			
<b>Xe-135</b>	<b>649(198)</b>		<b>9.14(2) h</b>	<b>(4.1(12)E-27)</b>			
249.770	90	1.000-Xd3	12.9(4) h	5.1(21)E-27			
249.770	90	0.969-Xs5	15.1(20)h	3.6(15)E-27			
<b>Ba-140</b>	<b>28(2)</b>		<b>12.752(3) d</b>	<b>(5.59(19)E-27)</b>	<b>12.752(3) d</b>	<b>(3.73(32)E-27)</b>	
29.964	14.1	7.696-Xd6	6.4(16) d	8.7(16)E-27			
162.660	6.22	1.266-Xd4	6.2(14) d	6.97(44)E-27			
162.660	6.22	1.223-Cd4	12.0(8) d	7.3(17)E-27			
304.9	4.29	1.132-Cd2	10.70 d	5.16(47)E-27			
328.762	20.3	1.103-Xd4	20(8) d	5.4(8)E-27			
328.762	20.3	1.241-Cd3	16.1(2) d	6.59(47)E-27			
423.75	3.15	1.025-Cd4	8.5(2) d	5.96(59)E-27	10.3(2)d	4.67(93)E-27	Cd4
487.021	45.5	1.064-Xd4	21(9)	5.4(7)E-27			
487.021	45.5	1.116-Cd4	16.1(2) d	5.06(20)E-27	11(4) d	5.58(53)E-27	Cd4
537.261	24.39	1.016-Xd4	11.4(2) d	5.72(41)E-27			
537.261	24.39	1.040-Cd4	13.4(1) d	5.93(32)E-27	11(3) d	4.08(63)E-27	Cd4
815.7	23.28	0.993-Cd4	17(4)d	5.55(79)E-27	11.02(4)d	4.67(63)E-27	Cd4
867.8	5.50	1.047-Cd2	—	5.90(83)E-27	3.37d	3.53(10)E-27	Cd2
1596.210	95.4	1.125-Cd4	17(3) d	4.58(55)E-27	13(4) d	7.75(67)E-27	Cd4
<b>Ce-141</b>	<b>10.0(3)</b>		<b>32.501(5)d</b>	<b>(5.65(13)E-27)</b>	<b>32.501(5)d</b>	<b>(3.88(44)E-27)</b>	
145.441	48.2	1.275-Xd6	44(7)d	5.53(16)E-27	—	4.31(16)E-27	Xd5
145.441	48.2	1.136-Xs7	65(18)d	5.65(40)E-27	39(10)d	3.26(13)E-27	Xs7
145.441	48.2	1.275-Cd3	30.7(25)d	5.93(24)E-27	20(10)d	4.70(20)E-27	Cd4

Table 2. Continuation

Isotope $E_\gamma$ [keV]	Activity [Bq] $I_\gamma$ [%]	$\eta$ -XsM $\eta$ -CdM	a hole		b hole		XsM CdM
			$T_{1/2}$ (Lib.) $T_{1/2}$ (Exp.)	$\langle R \rangle$ R	$T_{1/2}$ (Lib.) $T_{1/2}$ (Exp.)	$\langle R \rangle$ R	
<b>Ce-143</b>	<b>222(5)</b>		<b>33.039(6) h</b>	<b><math>\langle 6.49(10)E-27 \rangle</math></b>	<b>33.039(6) h</b>	<b><math>\langle 3.44(18)E-27 \rangle</math></b>	
57.356	11.7	1.456-Xs6	42.7(19) h	1.18(4)E-26*	38.4(6) h	1.41(6)E-26*	Xs5
57.356	11.7	1.900-Xd5	39.6(12) h	1.34(11)E-26*	38.4(6) h	1.12(4)E-26*	Xd5
293.266	42.8	1.021-Xs6	32.4(10) h	6.54(19)E-27	31.2(05) h	2.80(9)E-27	Xs3
293.266	42.8	1.054-Xd2	32.2(6) h	6.63(19)E-27	35.04(4) h	3.39(12)E-27	Xd4
293.266	42.8	1.044-Cd4	37.2(4) h	6.6(14)E-27	40.2(4) h	3.45(6)E-27	Cd3
350.98	3.23	0.828-Xs3	41(12) h	7.3(9)E-27			
350.98	3.23	0.850-Xd3	89(19) h	7.4(7)E-27			
664.571	5.69	1.026-Xd1		6.11(17)E-27			
664.571	5.69	0.986-Cd4	16.16(17) h	6.27(79)E-27			
721.86	5.39	0.970-Cd2	70.56h	5.3(17)E-27	—	3.74(6)E-27	Cd2

Note: Averaging is done without including the data marked with sign (\*). Activities are calculated for U sample with mass 0.1723 g and assuming the start of measurement time to be the end of irradiation.

in the aforesaid Tables. In these Tables, results in the bold face correspond to the upper variable of the heading which itself is shown in bold face. In the two Tables, for example, average value of all the observed peaks is given in bold face and the later values corresponding to individual peak are given in normal face.

From the data displayed in Tables 1 and 2 the following observations can be made:

The total number of spectra of  $^{232}\text{Th}$  and  $^{\text{nat}}\text{U}$  samples analyzed to obtain the above results are 33 and 22, respectively, for all the three holes «a», «b» and «c», and several hundreds of gamma ray peaks belonging to these spectra are analyzed. After the complete analysis for  $^{\text{nat}}\text{U}$  in the holes «a» and «b», 11 fission products namely,  $^{85\text{m}}\text{Kr}$ ,  $^{93}\text{Y}$ ,  $^{99}\text{Mo}$ ,  $^{103}\text{Ru}$ ,  $^{105}\text{Rh}$ ,  $^{131}\text{I}$ ,  $^{132}\text{Te}$ ,  $^{133}\text{I}$ ,  $^{140}\text{Ba}$ ,  $^{141}\text{Ce}$ , and  $^{143}\text{Ce}$  are observed along with  $^{239}\text{Np}$  as a result of  $(n, \gamma)$ , and  $^{237}\text{U}$  as a result of  $(n, 2n)$  reaction. In the previous experiment using the E + T assembly [23],  $^{237}\text{U}$  was not observed. For  $^{232}\text{Th}$  in the hole «a», total 6 fission products,  $^{85\text{m}}\text{Kr}$ ,  $^{99}\text{Mo}$ ,  $^{131}\text{I}$ ,  $^{133}\text{Xe}$ ,  $^{135}\text{Xe}$ , and  $^{141}\text{Ce}$  are observed along with  $^{233}\text{Pa}$ , i.e., daughter elements produced in decay of  $^{233}\text{Th}$  as a result of  $^{232}\text{Th}(n, \gamma)$  reaction and  $^{231}\text{Th}$  as a result of  $^{232}\text{Th}(n, 2n)$  are also observed. For  $^{232}\text{Th}$  in the hole «b», all the above mentioned fission products (except  $^{99}\text{Mo}$ ,  $^{133}\text{Xe}$ ,  $^{135}\text{Xe}$ ) along with  $^{233}\text{Pa}$  and  $^{231}\text{Th}$  are observed. Lastly, in the case of the hole «c» only  $^{99}\text{Mo}$  is observed as a fission product and  $^{233}\text{Pa}$  as an  $(n, \gamma)$  product. One important observation is that there is consistency in the reaction rates corresponding to the different gamma peaks of the same decaying nuclide. Discussion and comparison of these observations with the results of other experiments is being postponed for Section 6.

## 5. MONTE CARLO SIMULATIONS

**5.1. Simulation of Neutron Flux at Sample Positions.** Monte Carlo code MCNPX v2.6.C package of cascade model INCL4/ABLA and LA150 library is used [6] for the simulation of production of neutrons in collision of 2.33 GeV deuteron on the lead target and their transport in the graphite setup. As mentioned earlier, the  $^{232}\text{Th}$  samples were irradiated in all the three holes namely «a», «b» and «c» while the samples of  $^{\text{nat}}\text{U}$  were irradiated in holes «a» and «b» at the positions as shown in Fig. 1. The results of simulated neutron flux ( $E d\phi/dE$ ) per incident deuteron falling on the samples of  $^{232}\text{Th}$  and  $^{\text{nat}}\text{U}$  for the given positions in holes «a», «b» and «c» are given in Fig. 4. It can be seen clearly from the figures that there are low- and high-energy humps in the fluxes and the low-energy hump being pronounced shows that the graphite is a good moderator. It may also be noted that at all energies, neutron flux decreases from hole «a» to «c» because the distance of holes from the centre of the Pb-target increases gradually.

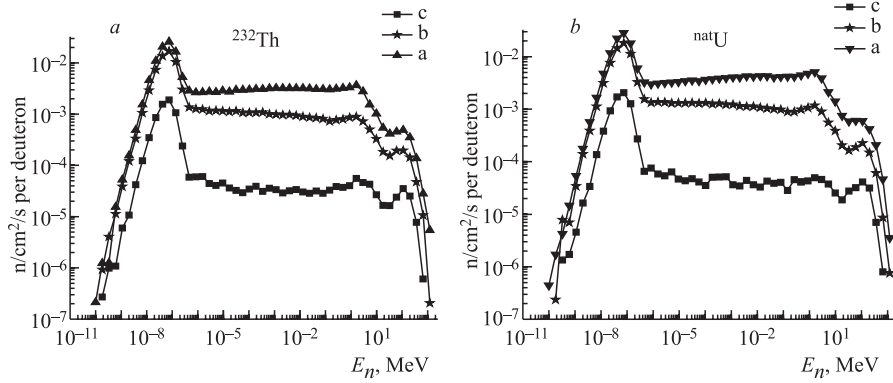


Fig. 4.  $E d\phi/dE$  per incident deuteron versus neutron energy,  $E_n$  at the position of  $^{232}\text{Th}$  sample (a) and  $^{\text{nat}}\text{U}$  sample (b) in holes «a», «b», and «c» simulated using Monte Carlo MCNPX code without the presence of the sample in the hole

**5.2. Calculation of Reaction Rates Using the Neutron Flux.** After simulation of the neutron flux at the positions of the samples, spectrum average cross sections for  $(n, \gamma)$ ,  $(n, 2n)$ , and  $(n, f)$  reactions are estimated using the pre-processing code NJOY 99.112 and the JEFF-3.1 nuclear data library [33] for the cross sections of  $(n, \gamma)$  and  $(n, f)$  reactions. Cross sections of  $(n, 2n)$  reaction are taken from the MCNPX code itself. Total reaction rate is calculated by summing the partial reaction rates,  $R(A_r, Z_r, E_n)$  for all the energies from the thermal to the highest energy corresponding to the beam energy.

## 6. ANALYSIS OF RESULTS AND CONCLUSIONS

**6.1. Determination of Group Weight Factors for Calculation of Total Number of Fissions.** Samples of  $^{\text{nat}}\text{U}$  and  $^{232}\text{Th}$  are placed at different positions in the three holes therefore the fission takes place differently due to (i) neutron flux is different in these positions, (ii) the rate of the fission of  $^{235}\text{U}$  differs from that of  $^{238}\text{U}$  and (iii) all the fission products may not be observed in the experiment. In this situation, the measured production rate of a fission product needs to be converted into the total fission rate. As an approximation, we may know the weight factors of the fission as functions of neutron energy and the position in a setup. For the fission reaction rate  $R(t, r, E_n)$  we have the next meanings of symbols in brackets: neutrons of energy  $E_n$  ranging from thermal to maximum projectile energy on interacting with target; «t» — produced fission product, «r» — corresponding to the cumulative yield  $Y(t, r, E_n)$  of the said product. Thus the

measured rate,  $R_{\text{exp}}(t, r) = \sum_{E_n} R(t, r, E_n)$  corresponds to the mean cumulative yield  $Y_{\text{cum}}(t, r)$ . In the case of the  $^{235}\text{U}$  data, both the independent yield and the cumulative yields are available at 0.025 eV, 400 keV and 14 MeV. However, for  $^{238}\text{U}$  and  $^{232}\text{Th}$  the data are available for 400 keV and 14 MeV. Thus, the full range of neutron energy is divided into the following three ranges and it is assumed that  $Y_{\text{cum}}$  stays roughly constant in these ranges:

- thermal, epithermal and resonance from 1E-5 eV to 1.26E+5 eV,
  - unresolved resonance and fast neutrons from 1.26 E+5 eV to 4.57 E+6 eV
- and
- fast and high-energy neutrons from 4.57 E+6 eV to the beam energy, i.e., 2.33 GeV.

$Y_{\text{cum}}(t, r)$  for  $^{232}\text{Th}$  may be calculated using the following relation:

$$Y_{\text{cum}}(^{232}\text{Th}, r_1) = w_2(\text{Th}), Y_{\text{cum}}(^{232}\text{Th}, r_1, 2) + w_3(\text{Th}), Y_{\text{cum}}(^{232}\text{Th}, r_1, 3), \quad (3)$$

where  $r_1 = {}^{85m}\text{Kr}, {}^{99}\text{Mo}, {}^{131}\text{I}, {}^{133}\text{Xe}, {}^{135}\text{Xe}$  and  ${}^{141}\text{Ce}$  for  $^{232}\text{Th}$ .

The weight factor,  $w_j$  is defined as a fraction of a fission reaction rate in the  $j$ th energy range. This is calculated using the JEFF-3.1 data library of fission cross sections and the neutron flux in different positions of say  $^{232}\text{Th}$  in the three holes. For the composite targets like  $^{\text{nat}}\text{U}$  for accounting for the abundance of isotopes the following relation is used:

$$Y_{\text{cum}}(t, r) = \sum_{i,j} a_i w_{ij} Y_{\text{cum}}(i, j, r)$$

Table 3. Group weight factors  $w_j$  for the calculations of total number of fissions

Range of neutron Energy, $j$	$^{232}\text{Th}$	$^{235}\text{U}$	$^{238}\text{U}$	$^{\text{nat}}\text{U}$
<b>Hole a</b>				
Epithermal	4.24E-06	0.9377	3.301E-05	0.9377
Resonance	0.285	9.063E-04	2.087E-02	2.178E-02
Fast	0.715	3.972E-04	3.992E-02	4.032E-02
<b>Hole b</b>				
Epithermal	3.38E-06	0.9721	2.696E-06	0.9721
Resonance	0.225	3.296E-04	7.874E-03	8.204E-03
Fast	0.775	1.902E-04	1.953E-02	1.955E-02
<b>Hole c</b>				
Epithermal	1.01E-06	0.9737	1.090E-05	0.9737
Resonance	0.133	1.231E-04	3.123E-03	3.246E-03
Fast	0.869	2.055E-04	2.285E-02	2.289E-02

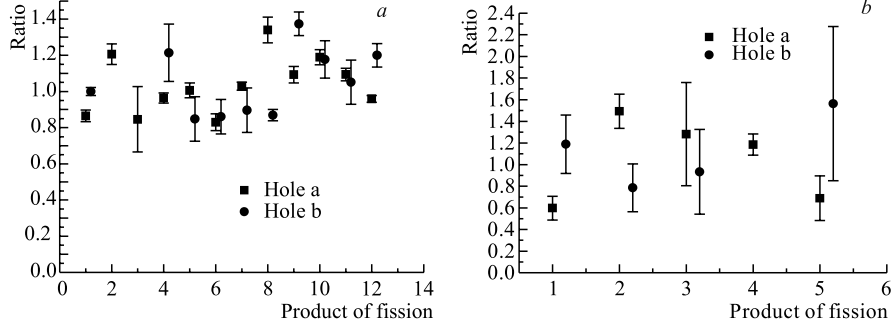


Fig. 5. *a)* The ratio  $(R_{\text{exp}}(^{\text{nat}}\text{U}, r)/Y_{\text{cum}}(^{\text{nat}}\text{U}, r))$  for the 11 fission products and *b)*  $(R_{\text{exp}}(\text{Th}, r)/Y_{\text{cum}}(\text{Th}, r))$  for 5 fission products normalized over the average of the ratio taken over  $\langle r \rangle$  is compared for corresponding fission fragments in holes «a» and «b»

The weight factors  $w_j$  for  $^{232}\text{Th}$  and reduced group factors,  $a_i w_{ij}$  for  $^{235}\text{U}$  ( $i = 1$ ) and  $^{238}\text{U}$  ( $i = 2$ ) are given in Table 3. The sum of group weight factors  $\sum w_j$  and  $\sum_{i,j} a_i w_{ij}$  is equivalent to one. In the case of  $^{\text{nat}}\text{U}$ ,  $a_1 = 0.0072$ , and then  $w_{1j}$  need to be calculated for  $^{235}\text{U}$  and  $a_2 = 0.9928$  for  $^{238}\text{U}$ , and  $w_{2j}$  need to be calculated as in the case of  $^{232}\text{Th}$  with  $r = ^{85m}\text{Kr}, ^{93}\text{Y}, ^{99}\text{Mo}, ^{103}\text{Ru}, ^{105}\text{Rh}, ^{131}\text{I}, ^{132}\text{Te}, ^{133}\text{I}, ^{140}\text{Ba}, ^{141}\text{Ce}$ , and  $^{143}\text{Ce}$  for  $^{\text{nat}}\text{U}$ .

Thus, the ratio,  $R/Y$  is estimated using values of the experimental reaction rate,  $R_{\text{expt}}(t, r)$  for the  $r$ -fission fragments and the mean cumulative production yield,  $Y_{\text{cum}}(t, r)$  as determined above. Normalization ratio,  $R/Y$  is plotted for  $^{\text{nat}}\text{U}$  and  $^{232}\text{Th}$  in the case of the holes «a» and «b» in Fig. 5. From these plots it is observed that for a given sample say  $^{\text{nat}}\text{U}$ , fission fragment ratio,  $R/Y$  stays roughly independent of the product, «r».

This in turn gives the reaction rate of fission. It is the well-known fact that the sum of independent yields is not equal to corresponding cumulative yield and the relation between them depends on the half-lives of the nuclei present in the decay chain [34]. A particular fission product  $(A_r, Z_r)$  may be produced in a fission reaction directly and the same  $(A'_r, Z'_r)$  may also appear on decay of another product. Also, it may also happen that some of them are not observed in the gamma-spectrometry because of their half-life, may be very short or very long. Thus, we can use the sum of independent yields,  $\sum_r Y_{\text{ind}}(t, r)$  instead of the cumulative yield if the decay corrections for the previous nuclide could be neglected and we calculate the total reaction rate for fission from all residual nuclei as follows:

$$R_{\text{exp}}(\text{fission}, t, r) = \frac{200 R_{\text{exp}}(t, r)}{\sum_{r'=1}^r Y_{\text{ind}}(t, r')} = \frac{200 R_{\text{exp}}(t, r)}{Y_{\text{cum}}(t, r)}.$$

Table 4. Comparison of experimentally measured (E) and calculated (C) reaction rates in the three holes. For the calculations JEFF 3.1 library is used

Hole a						
	<sup>232</sup> Th			natU		
Reaction	(n, γ)	(n, f)	(n, 2n)	<sup>238</sup> U (n, γ)	natU (n, f)	<sup>238</sup> U (n, 2n)
R <sub>expt</sub> (E)	3.20(8)E-25	1.40(19)E-26 1.70(29)E-26*	7.6(8)E-27	3.11(10)E-25	1.57(21)E-25	2.72(9)E-27
R <sub>cal</sub> (C)	7.83E-25	5.09E-27	3.27E-27	1.63E-24	2.54E-25	2.73E-27
E/C	0.409(10)	2.75(37)	2.33(25)	0.191(6)	0.618(83)	0.945(26)
Hole b						
	<sup>232</sup> Th			natU		
Reaction	(n, γ)	(n, f)	(n, 2n)	<sup>238</sup> U (n, γ)	natU (n, f)	<sup>238</sup> U (n, 2n)
R <sub>expt</sub> (E)	1.92(5)E-25	3.8(13)E-27 4.4(13) E-27*	3.6(18)E-27	2.08(20)E-25	1.02(12)E-25	7.21(20)E-28
R <sub>cal</sub> (C)	4.04E-25	1.78E-27	7.58E-28	6.07E-25	1.56E-25	7.63E-28
E/C	0.475(12)	2.1(7)	4.7(24)	0.343(33)	0.654(77)	0.945(26)
Hole c						
	<sup>232</sup> Th			natU		
Reaction	(n, γ)	(n, f)	(n, 2n)	<sup>238</sup> U (n, γ)	natU (n, f)	<sup>238</sup> U (n, 2n)
R <sub>expt</sub> (E)	3.38(16)E-26	5.1(18)E-28 5.1(18)E-28*	—	—	—	—
R <sub>cal</sub> (C)	3.39E-26	2.13E-28	6.84E-29	3.73E-26	1.79E-26	6.61E-29
E/C	0.997(47)	2.4(9)	—	—	—	—
*The values correspond to the values obtained on inclusion of data from TALYS code at higher than 14 MeV energy and the method of calculation is explained in Appendix A. In the discussions these values are not included as they are with large uncertainties and they are not purely from the experiment.						

The experimental values of R<sub>exp</sub> (fission) for <sup>232</sup>Th in holes «a», «b» and «c» and for natU in holes «a» and «b» are calculated. Averaging the value R<sub>exp</sub> (fission, t, r) of individual fission product we calculate the total fission rate, R<sub>exp</sub> (t, fission) and it is given in Table 4 for natU and <sup>232</sup>Th samples in their respective holes. The theoretical reaction rates are also calculated for all the observed reactions, i.e., (n, γ), (n, 2n), and (n, fission) for both <sup>232</sup>Th and natU samples in the holes «a», «b» and «c» using the Monte Carlo MCNPX, JEFF-3.1 and NJOY 99.112 codes, and displayed along with the experimental values in Table 4. Their discussion is postponed for the next section.

**6.2. Calculation of Transmutation Power.** The transmutation of <sup>232</sup>Th to <sup>233</sup>U and <sup>238</sup>U to <sup>239</sup>Pu by (n, γ) reactions can be written as the following decay chains:

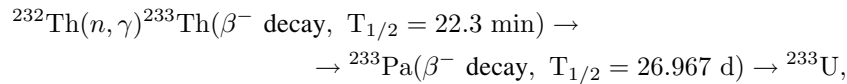
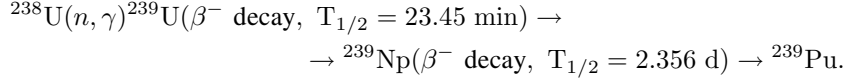
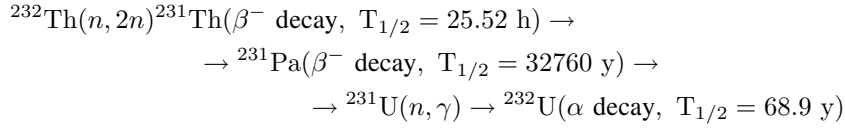


Table 5. Comparison of normalized transmutation power  $P_{\text{norm}}$  of three assemblies namely Graphite-lead target, Energy plus Transmutation (Pb target and U blanket) and TARC. Distances of the samples from the centre of their respective assemblies are given as «d»

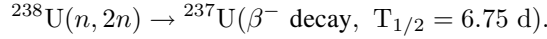
Assembly	Graphite			E+T	TARC	
	Hole a	Hole b	Hole c			
Distance «d» (Th)	d ~ 24cm	d ~ 34 cm	d ~ 61 cm	d ~ 13 cm	Z = 22.5 cm, X = 122 cm	Z = 7.5 cm, X = 150 cm
$^{232}\text{Th}(n,\gamma) \rightarrow ^{233}\text{Pa}$	3.21(8)E-16	1.93(5)E-16	3.39(16)E-17	3.09(13)E-17	3.8(3)E-17	1.0(2)E-17
$^{232}\text{Th}(n,2n) \rightarrow ^{231}\text{Th}$	7.6(8)E-18	3.6(18)E-18	—	1.59(16)E-18	—	—
Distance «d» (U)	d ~ 19 cm	d ~ 31 cm	d ~ 58 cm	d ~ 13 cm	Z = -22.5 cm, d = 107 cm	Z = -22.5 cm, d = 94 cm
$^{238}\text{U}(n,\gamma) \rightarrow ^{239}\text{Np}$	3.12(10)E-16	2.09(20)E-16	—	2.87(9)E-17	1.1(3)E-17 Hole 6	7.7(2)E-17 Hole 7
$^{238}\text{U}(n,2n) \rightarrow ^{237}\text{U}$	2.71(9)E-18	7.18(20)E-19	—	—	—	—



Similarly for the  $(n, 2n)$  reactions in case of  $^{232}\text{Th}$  and  $^{238}\text{U}$ ,



and for the uranium,



In the experiment, product nuclides  $^{233}\text{Pa}$ ,  $^{231}\text{Th}$ ,  $^{239}\text{Np}$ , and  $^{237}\text{U}$  have been observed and  $P_{\text{norm}}$  has been estimated using Eq. (2) of Section 3 corresponding to the  $(n, \gamma)$  and  $(n, 2n)$  reactions of  $^{232}\text{Th}$  and  $^{\text{nat}}\text{U}$  samples for the holes «a», «b», and «c» using the values of  $R_{\text{exp}}$  of Table 4. Results of  $P_{\text{norm}}$  of this experiment are displayed in Table 5 along with the results of other experiments viz. E + T [23] and the TARC [22] for the sake of comparison.

The following observations can be made from the experimental and theoretical results:

i) The experimental values of the reaction rates,  $R_{\text{expt.}}$  for all the three reactions, i.e.,  $(n, \gamma)$ ,  $(n, 2n)$ , and  $(n, \text{fission})$  for both  $^{\text{nat}}\text{U}$  and  $^{232}\text{Th}$  samples decrease as we go from the hole «a» which is closer to the target than the hole «c». This is because of the fact that the neutron flux gets moderated and its magnitude also decreases with the distance from the target.

ii) The ratio, E/C is reasonably close to the unity for the  $(n, f)$  and  $(n, 2n)$  reactions and for  $^{\text{nat}}\text{U}$  sample it is much less than unity in the case of  $(n, \gamma)$  reactions in both the holes «a» and «b» as well as for both the samples. In the case of  $^{232}\text{Th}$ , ratio,  $R(\text{expt.})/R(\text{cal})$  for both  $(n, f)$  and  $(n, 2n)$  reactions is not unity for the three holes. The reasons for this may be the lack of precise cross section library particularly at neutron energies greater than 20 MeV.

iii) For  $^{232}\text{Th}$  in the hole «a» the ratio of  $R_{\text{exp}}(n, 2n)/R_{\text{exp}}(n, f)$  is 54(10)% compared to  $R_{\text{theor}}(n, 2n)/R_{\text{theor}}(n, f) = 64.24\%$ . For the hole «b» the ratio  $R_{\text{exp}}(n, 2n)/R_{\text{exp}}(n, f)$  is 95(57)% compared to  $R_{\text{theor}}(n, 2n)/R_{\text{theor}}(n, f) = 42.84\%$ . This shows that agreement is reasonably good in both the cases.

iv) In the case of  $^{\text{nat}}\text{U}$ ,  $R_{\text{exp}}(n, 2n)/R_{\text{exp}}(n, f)$  is 1.73(20)% and  $R_{\text{theor}}(n, 2n)/R_{\text{theor}}(n, f)$  is 1.07% in hole «a» and for the hole «b» the ratio  $R_{\text{exp}}(n, 2n)/R_{\text{exp}}(n, f)$  is 0.710(9)% and  $R_{\text{theor}}(n, 2n)/R_{\text{theor}}(n, f)$  is 0.49%. It is evident that the ratio is very small in the case of hole «a» compared to hole «b» and the

reason is the presence of fissile component  $^{235}\text{U}$  in  $^{\text{nat}}\text{U}$  which has high fission cross section at lower neutron energies in the hole «b».

v) From the ratio of experimental reaction rates,  $^{\text{nat}}\text{U}(n, f)/^{232}\text{Th}(n, f)$  being 11.2(17) for the hole «a» and 26.8(85) for the hole «b» it is clear that there is more flux of the moderated neutrons in the hole «b» than in the hole «a» which enhances the fission rate of  $^{235}\text{U}$ . In another way,  $^{\text{nat}}\text{U}(n, f)_b/^{\text{nat}}\text{U}(n, f)_a \sim 0.65(12)$  and  $\text{Th}(n, f)_b/\text{Th}(n, f)_a \sim 0.27(10)$  also support the aforesaid view that there is bigger component of slowed down neutrons in the hole «b» than in the hole «a».

vi) Similarly, the ratio of the experimental reaction rates  $^{238}\text{U}(n, 2n)/^{232}\text{Th}(n, 2n) = 0.36(4)$  for the hole «a» and 0.20(10) for the hole «b» shows that  $^{232}\text{Th}$  is more prone to the  $(n, xn)$  reaction than  $^{238}\text{U}$ .

The following observations can be made about the normalized transmutation power,  $P_{\text{norm}}$  (see Table 5 for the data) for both  $^{\text{nat}}\text{U}$  and  $^{232}\text{Th}$  in the three holes «a», «b» and «c»,

i)  $P_{\text{norm}}$  for both  $^{232}\text{Th}$  and  $^{238}\text{U}$  samples deduced using the rates of  $(n, \gamma)$  and  $(n, 2n)$  reactions decreases as we go from the hole «a» to «c», i.e., on increasing the distance,  $d$  from the centre of the spallation neutron source. This is because of the fact that both the flux and the energy decrease with the distance. It seems that the flux probably decreases much faster than the energy because the rate of  $(n, \gamma)$  reaction should not increase if alone the average energy had decreased.

ii) Transmutation power in the case of  $(n, \gamma)$  reaction for  $^{232}\text{Th}$  and  $^{238}\text{U}$  independently for the holes «a» and «b» is found comparable and when we compare with the E+T and TARC assemblies it is about an order of magnitude higher than both the E+T and TARC assemblies results.

iii) The value of  $P_{\text{norm}}$  in the case of  $^{232}\text{Th}(n, 2n)$  reaction is about 2.1(11) times higher in the hole «a» than in the hole «b» and in the case of  $^{238}\text{U}(n, 2n)$  it is about 3.77(11) times higher in the hole «a» than in the hole «b». The difference in ratio in the case of Th and  $^{238}\text{U}$  is not high and this is also clear from the data on cross sections given in Fig. 6 below.

iv) On comparing  $P_{\text{norm}}(n, 2n)$  for  $^{232}\text{Th}$  in the case of graphite with E+T assemblies, it may be pointed out that transmutation power is about 5 times higher in the graphite assembly than in the E+T assembly.

The neutron flux in the graphite assembly in positions of irradiations of  $^{232}\text{Th}$  and  $^{\text{nat}}\text{U}$  samples ranging from thermal energy to  $\sim 1000$  MeV shows that it is equivalent to neither the thermal nor the fast reactor flux. In this range of energy three kinds of reactions  $(n, \gamma)$ ,  $(n, f)$ , and  $(n, 2n)$  have been observed in both samples of  $^{232}\text{Th}$  and  $^{\text{nat}}\text{U}$ . Because of the small neutron flux and small amounts of the two samples we have missed to observe the higher order  $(n, xn)$  reactions. In this experiment graphite has been used as a moderator while in the TARC experiment lead is a moderator as well as it works as the neutron multiplier

by way of  $(n, xn)$  kind of reactions. Thus, simulation of the neutron flux by a code is expected to be more cleaner in the case of graphite than of the lead due to the fact that lesser uncertainty is involved from the point of cross sections of high-order  $(n, xn)$  reactions.

Another important point about our experiment is that reaction rates deduced from different gamma peaks show consistency, and we have taken averages of the reaction rates with the help of only the singular gamma peaks without any interference of other elements.

Transmutation power of the setup is obtained using the two transmutation reactions namely  $(n, \gamma)$  and  $(n, 2n)$  and compared with the results of the E+T and the TARC setups considering reaction rates at the closest possible distances in the three experiments.

From the data on the rates of  $(n, 2n)$  and  $(n, f)$  reactions in the three positions of holes it may be inferred that the two reactions seem to be complimentary, i.e., in certain neutron environment if reaction rate of  $(n, f)$  increases, then reaction rate of  $(n, 2n)$  decreases and at the same time the rate of  $^{232}\text{Th}(n, 2n)$  reaction is more than that of the  $^{238}\text{U}(n, 2n)$  reaction. The effect was first pointed out in the simulation data of the CASCADE code in the case of the fertile and the fissile materials [35].

**Acknowledgements.** Authors are grateful to the operation crew of the Nuclotron accelerator of LHEP, JINR Dubna for irradiation and good beam parameters and to Dr. Vera Bradnova for managing support and preparing minutes of the experiment. Authors are also grateful to META Centrum (Czech Republic) for offering computers for the calculations. The experiments were supported by the Czech Committee for the collaboration with JINR, Dubna. Part of this work has been supported by grant of BRNS (DAE-India) and Indo-Russian ILTP and RFFI 09-02-92670 project grants .

## APPENDIX A

From the data of weight factors given in Table 3 the group weight factor for  $^{232}\text{Th}$  is dominant in the case of fast neutron energy for all three holes. We also understand that the cross sections for  $^{232}\text{Th}(n, f)$  reaction are the highest in this neutron energy interval. Since, there is no precise and systematic experimental data available for the independent and cumulative yields of fission products in the case of high-energy neutrons,  $E_n > 14$  MeV, so, we have used TALYS for

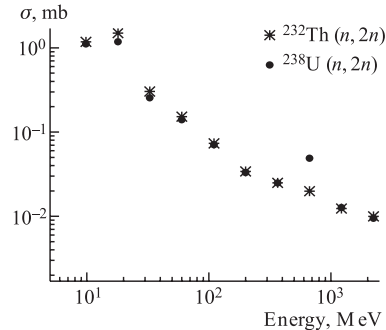


Fig. 6. Comparison of cross sections of  $^{232}\text{Th}(n, 2n)$  and  $^{238}\text{U}(n, 2n)$  reactions

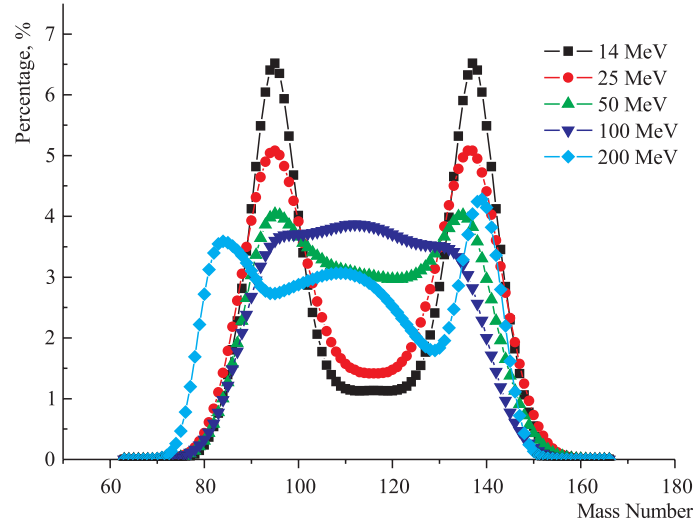


Fig. A1. Mass distribution of fission products of  $^{232}\text{Th}$  at five neutron energies calculated using the TALYS code

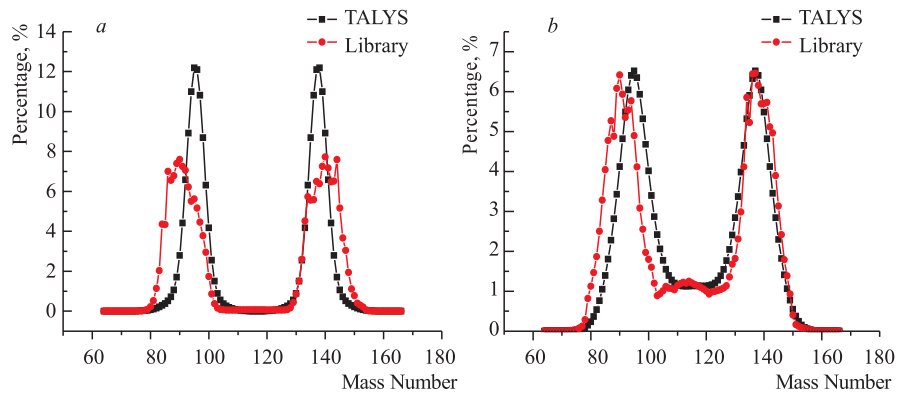


Fig. A2. Comparison of mass distribution of fission products from the TALYS code and the library in the case of a) 400 keV and b) 14 MeV energies

calculating the cross section and the independent yields of fission products for the energies  $E_n = 0.001, 0.01, 0.1, 0.4, 1.5, 10, 14, 20, 25, 35, 50, 75, 100, 150, 200$  MeV in the case of  $^{232}\text{Th}$  and other actinides.

In Fig. A1, the mass distribution of fission products in  $^{232}\text{Th}(n, f)$  reaction is given at few energies of neutrons and in Fig. A2 a comparative study of mass distribution of fission products from the calculated using cross sections from the TALLYS code and the experimental (library) is shown at the two energies, i.e.,  $E_n = 400$  keV and 14 MeV. It is clear from Fig. A2 that at 400 keV, large discrepancy is observed between the calculated and the experimental values, however, at 14 MeV the agreement is much better. We can assume that such situation may also exist in comparison of experimental and calculated values of the sum of independent yields in the corresponding chain products at the two energies.

In this way, we calculated the group weight factors at energies  $> 14$  MeV and listed them in Table A1. Summing over all the independent yields of nuclides preceding the decay chain of measured fission product, the equivalence  $Y_{\text{cum}}(^{232}\text{Th}, r) = \sum_{r'=1}^r Y_{\text{indep}}(^{232}\text{Th}, r')$  will also hold true. Since yield for the isomeric state is impossible to know from the TALYS code, so we have not included the contribution of  $^{85m}\text{Kr}$  like nuclide in the present calculation and also the contribution from  $^{135}\text{Xe}$  is not presently included because the cumulative yield is not equivalent to the sum of corresponding independent yields due to large uncertainties in decay of nuclides in the chain .

From the data in Table A1 it is clear that  $w_j$  are significantly high at higher energies and division of range of neutron energy may enhance accuracy in our calculations compared to when we consider a very big range of energies.

In the following Table A2, sum of independent yields is given for the five sets of energy values for the four observed fission products. In the last column ratio of the value at 14 MeV obtained from TALYS code to the value available in the data library is given for showing difference in the two values. The values given in columns 4, 5, and 6 are normalized with respect to the ratio given in the last column.

**Table A1. Group weight factors  $w_j$  calculated for the range of energy given in column 1 and in column 2, those neutron energies are given for which yield is calculated using data from TALYS code for the  $^{232}\text{Th}$ . In columns 3, 4, and 5 calculated weight factors are given for the three holes**

Ei-En [MeV]	Ej [MeV]	Hole a	Hole b	Hole c
1.00E-10 - 0.157	2.52E-08	1.95E-06	5.62E-06	6.02E-06
0.157 - 5.28	0.400	0.162	0.267	0.338
5.28 - 32.8	14	0.322	0.419	0.377
32.8 - 60	35,50	0.076	0.058	0.069
60 - 125	75,100	0.123	0.083	0.076
125 - 2.33E03	150, 200	0.316	0.172	0.140
Sum		1.000	1.000	1.000

**Table A2. Sum of independent yields up to the fission product, «r» of  $^{232}\text{Th}$  taken at different energies of neutrons. In the case of TALYS data average corresponding to the given set of energies is displayed**

r	0.4 MeV (library)	14 MeV (library)	35, 50 MeV (TALYS)	75, 100 MeV (TALYS)	150, 200 MeV (TALYS)	Normalization factor at 14 MeV TALYS/library
$^{99}\text{Mo}$	2.919	1.953	1.614	1.543	1.395	2.391(120)
$^{131}\text{I}$	1.513	2.306	2.520	2.075	1.582	1.470(87)
$^{133}\text{Xe}$	4.532	4.115	3.574	3.256	2.269	1.133(57)
$^{141}\text{Ce}$	7.106	5.722	3.567	2.339	3.079	0.844(57)

**Table A3. Deduced reaction rate of fission of  $^{232}\text{Th}$  using the experimental data on yields from the library at 400 keV and 14 MeV**

Fission product	Hole a $R_{\text{exp}} \times E-28$	Hole b $R_{\text{exp}} \times E-28$	Hole c $R_{\text{exp}} \times E-28$
$^{99}\text{Mo}$	190(42)	50(13)	5.0(18)
$^{131}\text{I}$	155(63)	132(58)	—
$^{133}\text{Xe}$	144(30)	—	—
$^{141}\text{Ce}$	97(34)	25(12)	—
Average	140(19)	38(21)	5.0(18)

**Table A4. Deduced reaction rate of fission  $^{232}\text{Th}$  using the experimental data on yields from library for the two neutron energies, 400 keV and 14 MeV and data of calculated yields for 35, 50, 75, 100, 150, and 200 MeV**

Fission product	Hole a $R_{\text{exp}} \times E-28$	Hole b $R_{\text{exp}} \times E-28$	Hole c $R_{\text{exp}} \times E-28$
$^{99}\text{Mo}$	236(32)	53(9)	5.1(18)
$^{131}\text{I}$	198(74)	142(56)	
$^{133}\text{Xe}$	194(42)		
$^{141}\text{Ce}$	118(52)	25(12)	
Average	170(29)	44(13)	5.1(18)

In the following Table A3, data on reaction rates deduced using the method given in Subsec. 6.1 and the data on the independent yield at two energies 400 keV and 14 MeV are presented for the fission of  $^{232}\text{Th}$  placed in the holes «a», «b» and «c». In the following Table A4 similar results are given on including the data on yields calculated from the TALYS code. It is important to point out that on inclusion of calculated data at higher than 14 MeV energies the reaction rates are enhanced  $\sim 21\%$  for example in case of hole «a».

In conclusion it may be stressed that there is need of getting more systematic experimental data at higher than 14 MeV neutron energies for the better calculations in the case of application of spallation neutrons for the ADS-like systems.

## REFERENCES

1. *Bowman C. D. et al.* // Nucl. Instr. Meth. A. 1992. V. 320. P. 336.
2. *Janssen A. J.* Transmutation of Fission Products in Reactors and Accelerator-Driven Systems, ECN-R-94-001. 2004.
3. *Rubbia C., Rubio J. A. et al.* Conceptual Design of a Fast Neutron Operated High Power Energy Amplifier CERN/AT/95-44 (ET). 1995. See also Rubbia C., A High Gain Energy Amplifier Operated with Fast Neutrons, AIP Conference 346, Proceedings of International Conference on Accelerator-Driven Transmutation Technologies and Applications, Las Vegas (NV), US. 1994.
4. Thorium Fuel Cycle — Potential Benefits and Challenges, IAEA-TECDOC-1450 (2005).
5. <http://www-nds.iaea.org/various1.htm>, [www-nds.iaea.org/](http://www-nds.iaea.org/), [www.nndc.bnl.gov/](http://www.nndc.bnl.gov/).
6. *Hendricks J. S. et al.* MCNPX, Version 2.6.c, LA-UR-06-7991. 2006.
7. <http://www.fluka.org/>
8. *Barashenkov V. S. et al.* CASCADE Program Complex for Monte-Carlo Simulation of Nuclear Processes Initiated by High Energy Particles and Nuclei in Gaseous and Condensed Matter. JINR preprint R2-85-173. Dubna, 1985;  
*Barashenkov V. S.* // Nucl. Phys. A. 1974. V. 231 P. 462;  
*Barashenkov V. S.* // Comp. Phys. Comm. 2000. V. 126. P. 28.
9. *Broeders C. H. M. et al.* FZK 7183 (2006);  
<http://bibliothek.fzk.de/zb/berichte/FZKA7183.pdf>
10. *Koning A. J. et al.* Proc. of the Intern. Conf. on Nuclear Data for Science and Technology, Santa Fe, USA, Sept. 26 – Oct. 1, 2004, [www.talys.eu](http://www.talys.eu).
11. *Shubin Yu. N. et al.* INDC (CCP) 385 (1995) Vienna;  
*Korovin Y. A. et al.* // Nucl. Instr. Meth. A. 2006. V. 562. P. 721.
12. *Kim G. N. et al.* // Nucl. Instr. Meth. A. 2002. V. 485. P. 458.
13. <http://pceet075.cern.ch/>
14. IREN Project. Intense Resonance Neutron Source. Compiled by A. K. Krasnykh, V. L. Lomidze, A. V. Novokhatsky, Yu. P. Popov, W. I. Furman. Frank Laboratory of Neutron Physics, JINR, Dubna, 1994.
15. <http://www.sckcen.be/myrrha/>
16. *Shvetsov V. et al.* // Nucl. Instr. Meth. Phys. Res. A. 2006. V. 562. P. 886.
17. *Krivopustov M. I. et al.* JINR Preprint P1-2000-168. Dubna, 2000;  
*Barashenkov V. S. et al.* // Nucl. Instr. Meth. Phys. Res. B. 2004. V. 217. P. 352.
18. <http://sinq.web.psi.ch/>

19. <http://www.kek.jp/intra-e/index.html>
20. <http://lansce.lanl.gov/indexC.shtml>
21. *Kim E. et al.* // Nucl. Sci. and Engineering. 1998. V. 129. P. 209–223.
22. *Abanades A. et al.* // Nucl. Instr. Meth. A. 2002. V. 478. P. 577.
23. *Adam J. et al.* JINR Preprint E15-2008-118. Dubna, 2008;  
*Adam J. et al.* // Eur. Phys. J. A. 2010. V. 43, No. 2. P. 159–173;  
*Krasa A. et al.* // Nucl. Instr. Meth. 2010. V. 615. P. 70.
24. *Adam J. et al.* // Kerntechnik. 2005. V. 70(3). P. 127.
25. *Adam J. et al.* Spallation Neutron Spectrum on a Massive Lead/Paraffin Target Irradiated with One GeV Protons // Euro. Phys. J. A. 2005. V. 23. P. 61.
26. *Titarenko Yu. E. et al.* // Phys. Rev. C. 2002. V. 65. P. 064610;  
*Titarenko Yu. E. et al.* // Phys. Rev. C. 2008. V. 78. P. 034615.
27. *Kumar V., Chitra Bhatia, Kumawat H.* CASCADE Data for the ADS Materials for Its Benchmarking // PSI Proceedings 09-01, ISSN 1019-0643, 30, 2009.
28. *Kumar V., Chitra Bhatia, Kumawat H., Adam J.* // Euro. Phys. J. A. 2009. V. 40 P. 231.
29. <http://www-nds.iaea.org/exfor>, Manish Sharma,  
*Kumar V. et al.* // Pramana J. Phys. 2007. V. 68. P. 307 with entries 33004001-20;  
*Adam J. et al.* // Kerntechnik. 2005. V. 70(3). P. 127 with entries from 3305001-5;  
*Kumar V. et al.* Paper Presented in NSRP-17 held at SINP Kolkatta on November 17–21, 2007 with EXFOR entries 33012001-7.
30. *Banaigs J. et al.* // Nucl. Instr. Meth. 1971. V. 95. P. 307.
31. *Frana J.* // J. Radioanal. Nucl. Chem. 2003. V. 257. P. 583–589.
32. *Chu S. Y. F., Ekstrom L. P., Firestone R. B.* <http://nucleardata.nuclear.lu.se>.
33. The JEFF-3.1 Nuclear Data Library, JEFF report 21 / Eds. A. Koning et al. ISBN 92-64-02314-3, Organization for Economic Co-Operation and Development, Nuclear Energy Agency, Paris, 2006.
34. *Adam J. et al.* // Applied Rad. Isotopes. 2002. V. 56. P. 607.
35. *Kumar V., Kumawat H., Chitra Bhatia* A Study of ADS Materials Using the CASCADE Code Presented at the IAEA Technical Meeting TM34567 on the Accelerator Simulation and Theoretical Modeling of Radiation Effects (SMoRE) held at Kharkov, Ukraine, June 9–13, 2008, and published on site <http://www-naweb.iaea.org/napc/physics/meetings/TM34567/login2.html>.

Received on May 26, 2011.

Редактор *Э. В. Ивашкевич*

Подписано в печать 13.10.2011.

Формат 60 × 90/16. Бумага офсетная. Печать офсетная.

Усл. печ. л. 1,94. Уч.-изд. л. 2,67. Тираж 345 экз. Заказ № 57457.

Издательский отдел Объединенного института ядерных исследований  
141980, г. Дубна, Московская обл., ул. Жолио-Кюри, 6.

E-mail: [publish@jinr.ru](mailto:publish@jinr.ru)

[www.jinr.ru/publish/](http://www.jinr.ru/publish/)